Intensified anticyclonic anomaly over the western North Pacific during El Niño decaying summer under a weakened Atlantic thermohaline circulation

Article

Published Version

It is advisable to refer to the publisher's version if you intend to cite from the work. See Guidance on citing.

Journal of Geophysical Research: Atmospheres

RESEARCH ARTICLE

Key Points:
- Investigate the change of WNPAC related to El Niño in water-hosing experiment
- Elucidate mechanisms for the intensified WNPAC under the weakened THC
- Demonstrate that enhanced El Niño and humidity result in intensified WNPAC

Correspondence to:
W. Chen,
chenwei@mail.iap.ac.cn

Intensified anticyclonic anomaly over the western North Pacific during El Niño decaying summer under a weakened Atlantic thermohaline circulation

Wei Chen[1], Riyu Lu[1], and Buwen Dong[2]

[1]State Key Laboratory of Numerical Modeling for Atmospheric Sciences and Geophysical Fluid Dynamics, Institute of Atmospheric Physics, Chinese Academy of Sciences, Beijing, China, [2]National Centre for Atmospheric Science-Climate, Department of Meteorology, University of Reading, Reading, UK

Abstract It has been well documented that there is an anticyclonic anomaly over the western North Pacific (WNPAC, hereafter) during El Niño decaying summer. This El Niño-WNPAC relationship is greatly useful for the seasonal prediction of summer climate in the WNP and East Asia. In this study, we investigate the modification of the El Niño-WNPAC relationship induced by a weakened Atlantic thermohaline circulation (THC) in a water-hosing experiment. The results suggest that the WNPAC during the El Niño decaying summer, as well as the associated precipitation anomaly over the WNP, is intensified under the weakened THC. On the one hand, this intensification is in response to the increased amplitude and frequency of El Niño events in the water-hosing experiment. On the other hand, this intensification is also because of greater climatological humidity over the western to central North Pacific under the weakened THC. We suggest that the increase of climatological humidity over the western to central North Pacific during summer under the weakened THC is favorable for enhanced interannual variability of precipitation, and therefore favorable for the intensification of the WNPAC during El Niño decaying summer. This study suggests a possible modulation of the El Niño–Southern Oscillation-WNP summer monsoon relationship by the low-frequency fluctuation of Atlantic sea surface temperature. The results offer an explanation for the observed modification of the multidecadal fluctuation of El Niño-WNPAC relationship by the Atlantic multidecadal oscillation.

1. Introduction

The lower tropospheric anticyclonic anomaly over the western North Pacific (WNP), which frequently persists from the El Niño mature winter to the following summer, is one of the key bridges that links El Niño and the East Asian summer monsoon [*Chang et al.*, 2000; *Wang et al.*, 2000; *Chou et al.*, 2003; *Wu et al.*, 2003; *Lau and Nath*, 2006]. *Wang et al.* [2000] suggested that the WNPAC is the response to the El Niño heating over the central and eastern equatorial Pacific and is maintained by local air-sea interaction. Some studies suggested that the anticyclonic anomaly over the western North Pacific (WNPAC) is the result of the suppressed convection over the Philippine Sea [*Lu*, 2001; *Lu and Dong*, 2001], which is caused by the change of mean sea surface temperature (SST) in the tropical Pacific [*Chang et al.*, 2000; *Wu and Wang*, 2002]. Recently, *Stuecker et al.* [2013] argued that the air-sea interaction is not essential for generating the WNPAC, because of it can be reproduced by an atmospheric general circulation model with prescribed SST change. Their results imply that atmospheric processes are also important to the WNPAC.

In addition, the Indian Ocean SST anomaly, following the wintertime El Niño events, contributes to the persistence of the WNPAC [*Watanabe and Jin*, 2002; *Yang et al.*, 2007; *Li et al.*, 2008; *Xie et al.*, 2009, 2010; *Chowdary et al.*, 2010, 2011; *Ding et al.*, 2010]. The strong positive Indian Ocean SST anomalies generate easterly flow extending to the western equatorial Pacific by inducing an atmospheric Kelvin wave, which therefore leads to a strong WNPAC. The capacitor effect of the Indian Ocean to the WNPAC plays an important role in prolonging the influence of El Niño–Southern Oscillation (ENSO) on the WNPAC [e.g., *Xie et al.*, 2009, 2010; *Chowdary et al.*, 2010].

It has been demonstrated that the strength of the WNPAC is associated with various ENSO activities. The increased magnitude and period of ENSO, which strengthens the monsoon-ocean interaction over the WNP, have resulted in a longer-lasting WNPAC during the ENSO decaying summer since the late 1970s [*Wang et al.*, 2008]. *Li et al.* [2007] pointed out that WNPAC strength is closely related to the amplitude of El Niño, according

to a coupled model results: a strong El Niño event leads to a strong WNPAC in the subsequent summer. *Chen et al.* [2012] demonstrated that both the strength of El Niño and the length of the decaying phase contribute to the intensity of WNPAC in the following summer. All of these studies mentioned that the strength of ENSO plays a key role in maintenance of the WNPAC.

ENSO strength is related to the changes of mean states in the tropical Pacific [e.g., *Gu and Philander*, 1995; *Wang and An*, 2002]. Some studies suggested that a remarkable change over the tropical Pacific occurs under the background of weakened Atlantic thermohaline circulation (THC) [e.g., *Dong and Sutton*, 2002; *Zhang and Delworth*, 2005; *Sutton and Hodson*, 2007; *Lu and Dong*, 2008]. *Dong and Sutton* [2007] indicated that this change manifests as warming in the southeastern tropical Pacific and the central equatorial Pacific and cooling in the northeastern tropical Pacific and the western Pacific. They further suggested that this change leads to an enhancement of ENSO variability by inducing westerly anomaly developed over the central Pacific, which results in an eastward shift of the ENSO coupled mode and Pacific warm pool. Additionally, the mean states of the Asian summer monsoon are suppressed by a weakened THC [*Zhang and Delworth*, 2005; *Lu and Dong*, 2008]. However, the ENSO-South Asian summer monsoon relationship is strengthened under the background of weakened THC, which corresponds to the changes of mean states over the tropical Pacific and the enhanced ENSO variability [*Lu et al.*, 2008].

In the present study, we focus on the changes of the WNPAC, representing the ENSO-WNP summer monsoon relationship, under the background of weakened THC. The results are obtained by comparing a water-hosing sensitivity experiment with the control run. The model and experiments are described in section 2. The El Niño-WNPAC relationship and its connection with Atlantic Ocean SST are first shown by observed evidence in section 3. The impacts of weakened THC on the WNPAC evolution associated with El Niño are demonstrated in section 4. The mechanisms for this change are discussed in section 5. The concluding remarks follow in section 6.

2. Model and Experiments

2.1. The Model

The model used in this study is a coupled atmosphere-ocean general climate model developed by the Hadley Centre (HadCM3). The atmospheric component of HadCM3 has 19 levels with a horizontal resolution of 2.5° latitude by 3.75° longitude [*Pope et al.*, 2000]. The oceanic component has 20 levels with a horizontal resolution of 1.25° by 1.25°. The two components were coupled once a day. The control simulation (CNTL) used preindustrial atmospheric trace gas concentrations and incoming solar radiation, providing only the external forcing and ran for 1000 years in which a stable climate is maintained without flux adjustments. The mean climate and its stability in the CNTL are discussed in *Gordon et al.* [2000]. Previous studies suggested that the model has a realistic representation of ENSO characteristics [*Collins et al.*, 2001; *AchutaRao and Sperber*, 2002; *Joseph and Nigam*, 2006], as well as the relationship between ENSO and Asian summer monsoon [*Li et al.*, 2007].

2.2. The Experiment

A water-hosing experiment that reveals the sensitivity of THC to an external source of freshwater [*Stouffer et al.*, 2006] was performed. The water-hosing experiment, hereafter referred to as 1 Sv (sverdrup; $1\,Sv = 10^6\,m^3\,s^{-1}$), is conducted in which an extra freshwater flux of 1.0 Sv ($1\,Sv = 10^6\,m^3\,s^{-1}$) was applied uniformly for 100 years to the North Atlantic Ocean surface between 50°N and 70°N. The initial conditions were taken from the 1000 years CNTL of the coupled model. The external freshwater forcing was then switched off after model year 100, and other 100 years integration continues. A 1.0 Sv freshwater flux leads to 70% weakening of THC in comparison with a steady strength in the CNTL [*Dong and Sutton*, 2007]. In the present study, the results of the first 100 years of the 1 Sv are compared with those of the 1000 years CNTL to assess the changes of the relationship between El Niño and WNPAC under a weakened THC. The same simulations have been used to investigate the impacts of weakened THC on ENSO variability [*Dong and Sutton*, 2007] and on the mean state of Asian summer monsoon [*Lu and Dong*, 2008] and on the ENSO-South Asian monsoon relationship [*Lu et al.*, 2008].

2.3. Response of SST to the Weakened THC in the 1 Sv

The weakened THC led to a significant change of mean states of SSTs globally. Figure 1 shows the response of climatological SSTs to the weakened THC during winter, spring, and summer. Over the Atlantic Ocean, SST was exhibited as an interhemispheric asymmetry with cooling in the North Atlantic (ranging from 1.0°C to
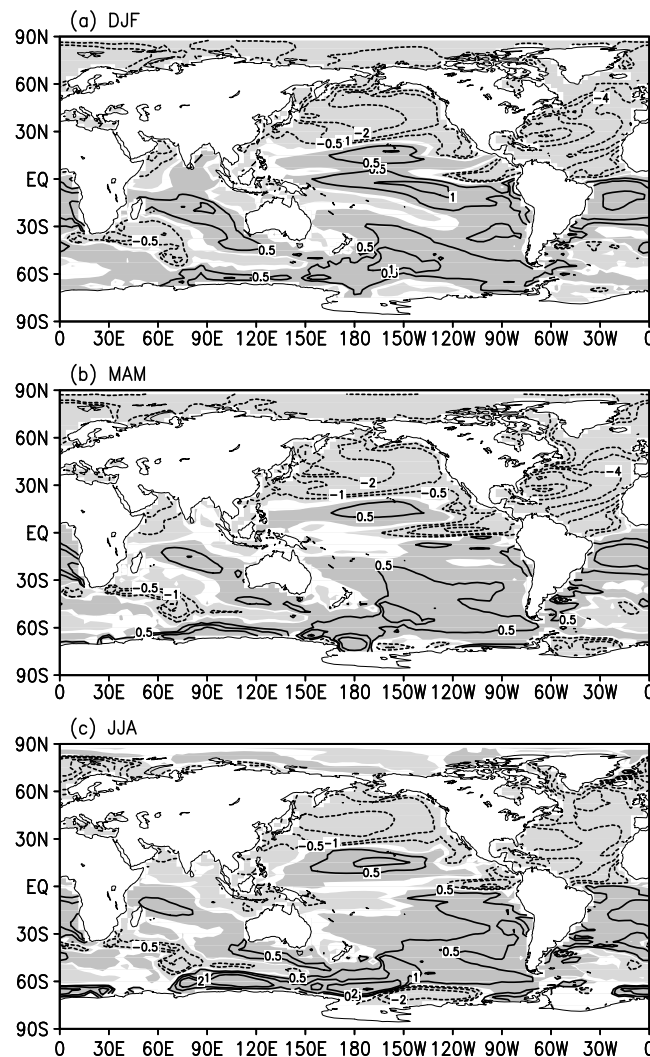
Figure 1. The differences of climatological seasonal mean sea surface temperature (SST; °C) between 1 Sv and CNTL experiments in (a) December-January-February (DJF), (b) March-April-May (MAM), and (c) June-July-August (JJA). Shading indicates regions in which the anomalies are significant at the 95% confidence level according to the t test. Contours are ±0.5, ±1.0, ±2.0, ±4.0, ±6.0, and ±8.0°C.

6.0°C) and a warming (approximately 1.0°C–2.0°C) in the South Atlantic, because of the pronounced decrease of northward ocean heat transport under the weakened THC [e.g., *Dong and Sutton*, 2002, 2007; *Dahl et al.*, 2005; *Zhang and Delworth*, 2005; *Timmermann et al.*, 2007]. These changes in SST existed in all three seasons and were strongest in winter (Figure 1a) and spring (Figure 1b) and slightly weak in summer (Figure 1c).

Furthermore, the weakened THC also induced significant remote responses outside the Atlantic. On the large scale, the response of SST showed a meridional dipole pattern with cooling over the Northern Hemisphere and warming over the Southern Hemisphere during all three seasons (Figure 1). However, SST increased in the northwestern to central tropical Pacific, which is consistent with that reported by *Dong and Sutton* [2007] and *Lu and Dong* [2008]. Our results further suggest that this significant warming is strongest in summer with an amplitude of approximately 1.0°C (Figure 1c), compared with 0.5°C in winter and spring (Figures 1a and 1b) when the largest warming occurs in the central and eastern tropical Pacific.

3. El Niño-WNPAC Relationship in Observations

In this study, an El Niño event is defined as December-January-February (DJF)-mean Niño 3 index larger than 1.0°C, in which the Niño 3 index defined as the SST anomalies averaged over 5°S–5°N,

90°–150°W. In observations, eight El Niño events were chosen under this criterion: 1957–1958, 1965–1966, 1972–1973, 1982–1983, 1986–1987, 1991–1992, 1997–1998, and 2009–2010.

Figure 2 shows the composite anomalies associated with El Niño events during their decaying summers in observations. These anomalies are characterized as positive SST anomalies over the central and eastern tropical Pacific and Indian Ocean (Figure 2a) and anticyclonic circulation and negative precipitation anomalies over the WNP (Figures 2b and 2c). This SST pattern contributes to an anticyclonic circulation over the WNP. In particular, the warm SST over the Indian Ocean works as a capacitor to maintain the WNPAC, which prolongs the influence of El Niño to the WNPAC [*Watanabe and Jin*, 2002; *Xie et al.*, 2009, 2010; *Li et al.*, 2010; *Chowdary et al.*, 2010, 2011].

The maintenance of the WNPAC and the associated negative precipitation anomaly over the WNPAC indicates the impact of El Niño decay in the WNP. The strong WNPAC is located over the South China Sea to the WNP. To measure the strength of the WNPAC, a WNPAC index is defined as the 850 hPa stream function averaged over the region 10°–25°N, 110°–160°E, shown by dashed rectangles in Figure 2
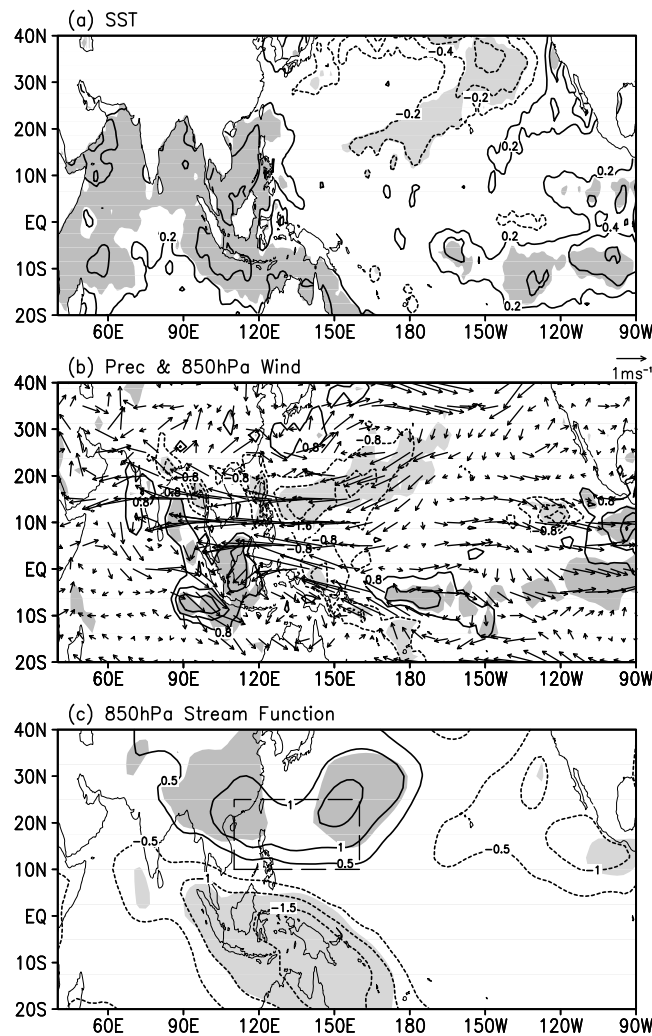
Figure 2. Composite of (a) SST (°C), (b) precipitation (contour; mm d^{-1}), (b) 850 hPa wind (vector), and (c) 850 hPa stream function anomalies (10^6 m^2 s^{-1}) for eight El Niño events in observations during the El Niño decaying summer June-July-August (JJA; 1). Shading indicates the region in which the anomalies are significant at the 95% confidence level according to the t test. The dashed rectangles represent the region defining the summertime western North Pacific anticyclone (WNPAC) index. The SST data are from the Hadley Centre sea ice and sea surface temperature (HadISST) [*Rayner et al.*, 2003] data sets from 1948 to 2013. The precipitation data are from Global Precipitation Climatology Project data set from 1979 to 2013. The circulation data are from the National Centers for Environmental Prediction/Department of Energy Reanalysis I data sets from 1948 to 2009 [*Kalnay et al.*, 1996].

(thisdefinition is according to the location of WNPAC in the model simulation). The WNPAC during the El Niño decaying summer in observations is 1.07×10^6 m^2 s^{-1}.

In observations, the fluctuation of SST over the Atlantic Ocean exhibited a low-frequency variability referred to as Atlantic multidecadal oscillation (AMO). Figure 3 illustrates that the multidecadal fluctuation of the El Niño-WNPAC rela tionship (blue line) essentially coincided with the phases of AMO (red line) such that a strong (weak) El Niño-WNPAC relationship occurred during a negative (positive) phase of AMO (i.e., weakened (intensified) THC). The correlation coefficient between the two time series of -0.34, which is significant at the 85% confidence level by the t test, implies a modulation of AMO on the El Niño-WNPAC relationship. This modulation is much clearer after the 1940s, with a correlation of -0.57 significant at the 98% confidence level. The data set is more reliable after that time due to the great increase in the total number of observational sea level pressure data [*Yin et al.*, 2008]. The correlation coefficient between the WNPAC and the Niño 3 index was 0.39 in 1968–1997 with a negative phase of AMO, in contrast with 0.20 in 1940–1967 with a positive phase of AMO.

Here we propose a hypothesis for the modulation of AMO to the El Niño-WNPAC relationship: The AMO affects the El Niño-WNPAC relationship by modifying the multidecadal fluctuation of ENSO intensity [e.g., *Dong et al.*, 2006; *Timmermann et al.*, 2007] and the climatological specific humidity over the western to central North Pacific. As shown in Figure 3, the multidecadal fluctuation of ENSO intensity and the climatological specific humidity have similar phase transitions as that for AMO. On the one hand, a negative (positive) phase of AMO is associated with a strong (weak) El Niño, leading to a strong (weak) El Niño-WNPAC relationship. On the other hand, the increase (decrease) in humidity over the western to central North Pacific, associated with a negative (positive) phase of AMO, is also favorable for a strong (weak) El Niño-WNPAC relationship.

The observed evidence implies a modulation of Atlantic Ocean to the El Niño-WNPAC relationship on the multidecadal timescale. Because of the lack of decadal samples in observations, we used model simulations to further investigate the physical mechanism to support our hypothesis.
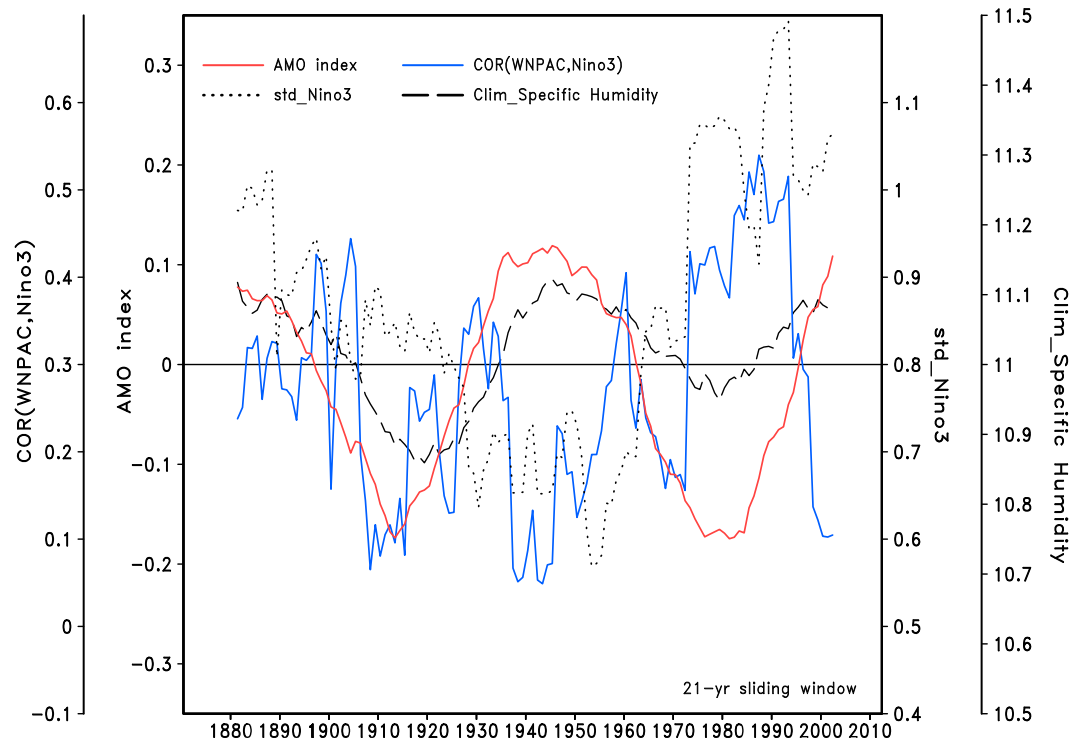
Figure 3. Time series of the Atlantic multidecadal oscillation (AMO) index with a 21 year running mean (red line; °C), the correlation coefficients between DJF-mean Niño 3 and JJA-mean WNPAC indices with 21 year sliding window (blue line), the 21 year sliding standard deviation of DJF-mean Niño 3 index (dotted line; °C), and the 21 year running mean of 850 hPa climatological specific humidity over the western to central North Pacific (dashed line; g kg^{-1}) in observations. The AMO index is defined as the annual mean SST anomalies averaged over the region of 0°–60°N, 7.5°–75°W. The specific humidity index is defined over the region of 10°–30°N, 120°–180°E. The SST data are from the Hadley Centre sea ice and sea surface temperature (HadISST) [*Rayner et al.*, 2003] data sets from 1870 to 2013. The circulation data are from the twentieth Century Reanalysis (20C) [*Compo et al.*, 2011] data sets from the same period.

4. Intensified WNPAC Under the Weakened THC

In the model simulations, an identical criterion as that used in observations was applied to choose the El Niño events for the two experiments. The threshold of 1.0°C is a slightly more (less) than 1 standard deviation in the CNTL (1 Sv). One hundred forty-two and twenty El Niño events were chosen in the 1000 years CNTL and 100 years 1 Sv, respectively.

Figure 4 shows the composite of 850 hPa stream function for the El Niño events from the mature winter D(0)JF(1) to the decaying summer June-July-August (JJA; 1). During D(0)JF(1) and spring March-April-May (MAM; 1), the strength and location of the WNPAC in the 1 Sv were similar to those in the CNTL, although the WNPACs were relatively stronger and occupied a larger area in the CNTL. The WNPACs in the two experiments developed in the El Niño mature winter D(0)JF(1) with the central area in the south extent of the South China Sea, and they further intensified with a slightly eastward shift in the following spring MAM(1).

The weakened THC manifested its influence on the WNPAC in JJA(1). For the CNTL, the WNPAC declined rapidly and moved to the central Pacific: only a weak circulation anomaly was noted over the WNP in JJA(1). In the 1 Sv, however, the WNPAC was well organized and strongly maintained over the WNP. The persistence of the summertime WNPAC in the 1 Sv indicates an intensified relationship between El Niño and the WNP summer climate under the weakened THC.

Figure 5 shows the evolution of WNPAC associated with the El Niño events for the two experiments. Here the 850 hPa stream function anomalies averaged over the rectangles marked in Figure 4 were used to measure the strength of WNPAC. Because the WNPAC moves eastward along with its evolution, the regions used to define the WNPAC index differ among seasons. To analyze the significance of the differences between the 1 Sv and the CNTL, we also showed the results in this figure as dots representing 10 periods, each including
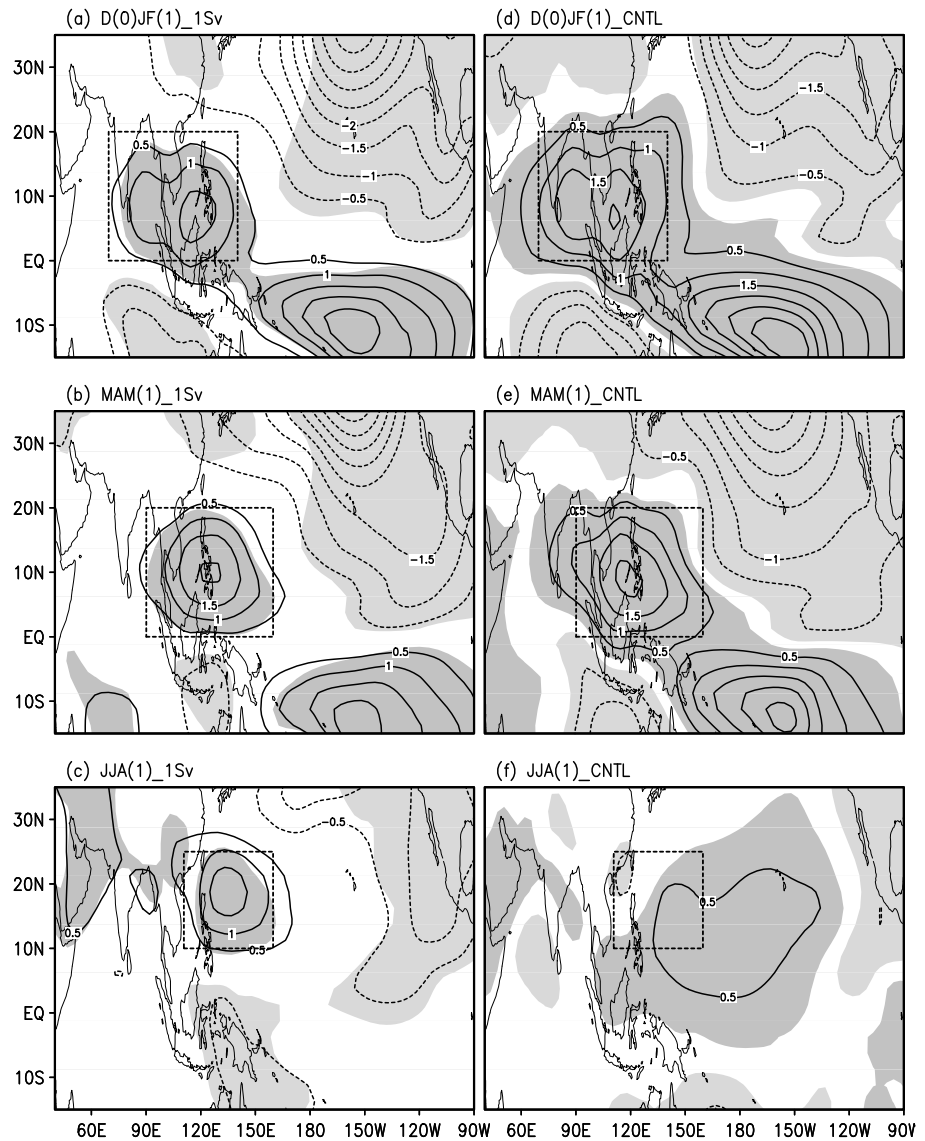
Figure 4. Composite of 850 hPa stream function anomalies ($10^6\,m^2\,s^{-1}$) for the El Niño events in the (a–c) 1 Sv and the (d–f) CNTL during the El Niño mature winter D(0)JF(1) to the decaying summer JJA(1). Shading indicates the region in which the anomalies are significant at the 95% confidence level according to the *t* test. The dashed rectangles represent the region defining the WNPAC index.

100 years of the 1000 years in the CNTL. These dots can be used to estimate the spread of WNPACs related to El Niño events in the CNTL. The numbers of El Niño events in these segments range from 11 to 18. All of the dots in D(0)JF(1) and MAM(1) indicated positive values, which confirms the existence of WNPACs in these seasons. In D(0)JF(1), the WNPAC was weaker in the 1 Sv in comparison with the CNTL. The robustness of this result is indicated because the WNPAC was weaker in the 1 Sv than that during all the segments in the CNTL. However, the WNPAC exhibited a similar intensity in MAM(1) for the CNTL and the 1 Sv, and the WNPAC intensity in the 1 Sv was among the spread between the segments in the CNTL. The difference between the WNPAC intensity in the 1 Sv and the mean in the CNTL was only $0.07 \times 10^6\,m^2\,s^{-1}$, although the WNPAC intensity ranged from $0.94 \times 10^6\,m^2\,s^{-1}$ to $1.35 \times 10^6\,m^2\,s^{-1}$ among the segments in the CNTL with a spread as high as $0.15 \times 10^6\,m^2\,s^{-1}$.

Again, the clearest difference appeared in JJA(1). The strength of the WNPAC in JJA(1) is $1.05 \times 10^6\,m^2\,s^{-1}$ for the 1 Sv, which is more than 4 times as strong as that for the CNTL ($0.23 \times 10^6\,m^2\,s^{-1}$). Furthermore, the strength of the WNPAC for the 1 Sv was stronger than any of the 100 years segments in the 1000 years CNTL,
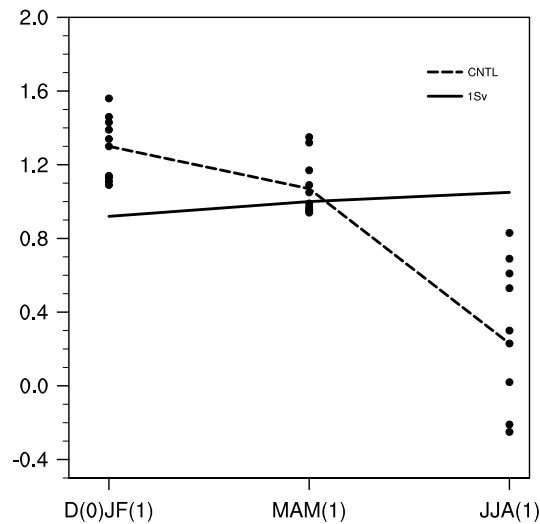
Figure 5. Composite evolution of WNPAC index for the El Niño events in the 1 Sv (solid line) and the CNTL (dashed line). Dots indicate 100 years segments in the 1000 years CNTL. The WNPAC index is defined as the 850 hPa stream function anomalies averaged over the region marked by rectangles in Figure 2 (0°–20°N, 70°–140°E in D(0)JF(1); 0°–20°N, 90°–160°E in MAM(1), and 10°–25°N, 110°–160°E in JJA(1)).

which indicates a robust intensification of WNPAC during El Niño decaying summer under the weakened THC. It should be noted that the intensification of WNPAC under the weakened THC did not depend on the definition of WNPAC. Same result can be obtained by using other definitions (results not shown).

The precipitation and lower tropospheric wind anomaly over the WNP in the El Niño decaying summer also showed difference between the two experiments (Figure 6). The significant negative precipitation anomaly over the WNP in the 1 Sv is associated with the strong summertime WNPAC. On the contrary, the WNP precipitation anomaly was significantly weaker in the CNTL, which is consistent with the weak circulation anomaly in that region. Thus, both the wind and precipitation over the WNP during the El Niño decaying summer were modulated by the weakened THC. However, positive SST anomalies over the Arabian Sea (Figure 2a) during the El Niño decaying summer were noted in observations. These warm SST anomalies led to an increase in moisture transport convergence and therefore precipitation over India despite a weakened monsoon circulation (Figure 2b) [*Chowdary et al.*, 2014]. In the CNTL, the positive SST anomalies over the Arabian Sea were weaker than those in observations [*Li et al.*, 2007], which led to a reduction in precipitation over India related to weaker monsoon circulation (Figure 6). This discrepancy indicates that the model has deficiency to simulate precipitation over India during El Niño decaying summer. Despite this deficiency over India, the large increase in precipitation over the Maritime Continent and the large decrease over the WNP during the El Niño decaying summer in the 1 Sv relative to the CNTL indicate a stronger impact of El Niño under the weakened THC.

5. Mechanisms for the Intensified WNPAC by the Weakened THC

5.1. Strengthened El Niño Intensity

Figure 7 shows the evolution of the probability for WNPAC occurrence in JJA (1) varying with the strength of El Niño in D(0)JF(1) for the 1000 years CNTL. The probability for WNPAC occurrence was increased along with the wintertime El Niño intensity. Among the El Niño events in which the D(0)JF(1) Niño 3 index was less than 1.5°C, slightly more than half (58%) were followed by the WNPACs in JJA(1); the remainder were followed by cyclonic anomalies over the WNP. When the D(0)JF(1) Niño 3 index was between 2.0°C and 2.5°C, the probability for WNPAC occurrence increased to 65%. Furthermore, when the D(0)JF(1) El Niño intensity is greater than 2.5°C, all of the El Niño events corresponded to the WNPAC in the subsequent summer. Thus, the summertime WNPAC is influenced by the wintertime El Niño intensity. Moreover, this influence strengthens along with the enhancement of El Niño intensity. These results still can be obtained by considering the spread among each 100 years segments in the 1000 years CNTL. The El Niño intensity plays a crucial role in the persistence of summertime WNPAC, which is consistent with that reported in previous studies [*Li et al.*, 2007; *Chen et al.*, 2012; *Stuecker et al.*, 2013]. In such studies, however, the role of El Niño intensity is investigated only by comparing the strong and moderate El Niño events. Our results further indicate that this role becomes stronger along with the enhancement of El Niño intensity.

Figure 8 shows the probability distribution of the DJF-mean Niño 3 index for the two experiments. The probability represents the proportion of El Niño events with D(0)JF(1) Niño 3 index in different strength bins among all integration years. For example, there are nine El Niño events with D(0)JF(1) Niño 3 index greater than 1.0°C but less than 1.5°C in the 100 years 1 Sv, so the probability for the bin between 1.0°C and 1.5°C is 9%.
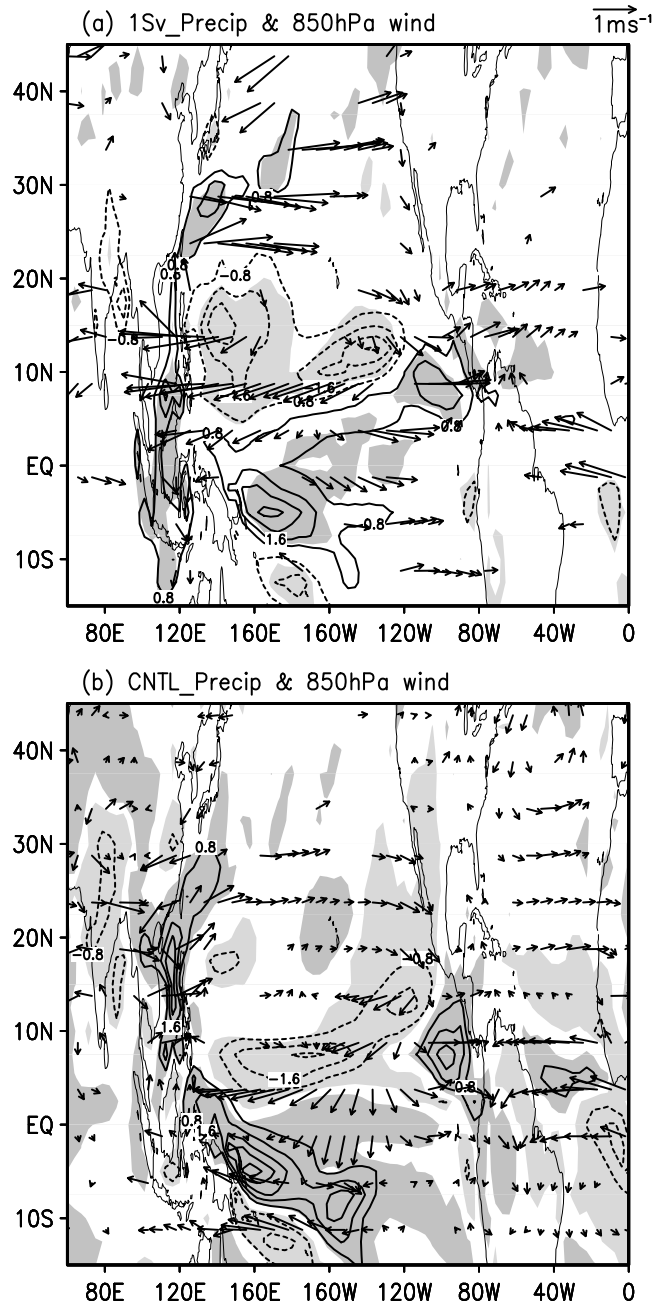
Figure 6. Same as Figure 2b but for precipitation anomalies (mm d^{-1}) and 850 hPa wind anomalies during JJA(1) in the (a) 1 Sv and the (b) CNTL. Shading indicates the region in which the precipitation anomalies are significant at the 95% confidence level according to the *t* test. For the 850 hPa wind anomalies, only those significant at the 95% confidence level are shown.

The same method is applied for the 1000 years CNTL. The probability between 1.0°C and 1.5°C for control run was 7.7%, which means that 77 El Niño events with D(0)JF(1) Niño 3 index greater than 1.0°C but less than 1.5°C.

Figure 8 indicates that the frequency of El Niño occurrence is higher in the 1 Sv, not only than that in the CNTL but also than the spread of 100 years segments in the 1000 years CNTL. Moreover, the frequency of El Niño events with a D(0)JF(1) Niño 3 index of more than 2.0°C is increased, which means that more strong El Niño events occurred under the weakened THC. Thus, both the occurrence frequency and amplitude for the El Niño events were enhanced under the weakened THC. Previous studies suggested that the ENSO variance is intensified by the weakened THC using different models [*Dong and Sutton*, 2007; *Timmermann et al.*, 2007], particularly noting the atmospheric teleconnection between the North Atlantic and tropical Pacific. Although *Timmermann et al.* [2005] argued that a weakened THC leads to a weakening of ENSO variability, they focused exclusively on the role of oceanic teleconnections, which is associated with a timescale of a few decades. Our results further demonstrate that the amplitude for individual El Niño event is also enhanced in the 1 Sv.

In addition, to further compare the strength of El Niño between the two experiments, all of the El Niño events are divided into categories of strong (with wintertime Niño 3 indices greater than 2.0°C) and moderate (with wintertime Niño 3 indices greater than 1.0°C but less than 2.0°C) ones. For all El Niño events, the wintertime intensity was stronger in the 1 Sv at 1.80°C than that in the CNTL at 1.64°C. Furthermore, the enhancement of intensity was mainly

contributed by strong rather than moderate El Niño events (Table 1), which implies that the intensification of the WNPAC by El Niño strength is induced by strong El Niño events.

Figure 9 shows the composite of the 850 hPa stream function is related to the strong El Niño events for the two experiments. The WNPACs shown in the figure are stronger than those associated with all El Niño events (Figure 2) during each season in both experiments, as was expected. In JJA(1), the WNPAC in the 1 Sv at $1.79 \times 10^6 \text{ m}^2 \text{ s}^{-1}$ was twice that in the CNTL at $0.86 \times 10^6 \text{ m}^2 \text{ s}^{-1}$. The intensification of the WNPAC associated
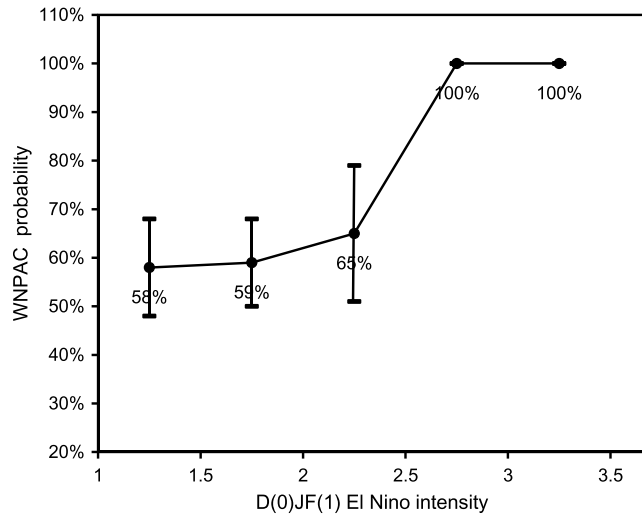
Figure 7. Evolution of probability of WNPAC occurrence varying with the D(0)JF(1) El Niño intensity in the CNTL. The WNPAC probability represents the proportion of the El Niño events followed by WNPAC among El Niño events with the D(0)JF(1) Niño 3 index between the certain values. The black bars represent the spread among the 100 years segments in the 1000 years CNTL.

with the strong El Niño events under the weakened THC further indicates the role of wintertime El Niño strength in affecting the summertime WNPAC.

5.2. Enhancement of Climatological Humidity Over the Western to Central North Pacific

Figure 10 shows the composite of the 850 hPa stream function related to the moderate El Niño events in the two experiments. The distributions of composite stream function anomalies were very similar to but significantly weaker than those related to the strong El Niño events in the two experiments shown in Figure 9. For the moderate El Niño events, the corresponding WNPACs during JJA(1) also showed an intensification in the 1 Sv (Figure 10); the WNPAC index was $0.80 \times 10^6 \, m^2 \, s^{-1}$ in the 1 Sv but only $0.03 \times 10^6 \, m^2 \, s^{-1}$ in the CNTL. The stronger WNPACs for the moderate as well as for the strong El Niño events under the weakened THC confirm the role of the weakened THC in strengthening the relationship between El Niño and the WNPAC.

However, the intensity of the moderate El Niño events cannot be used to explain the intensification of the WNPAC during JJA(1) in the 1 Sv. The wintertime intensity of moderate El Niño events was similar between the 1 Sv and the CNTL (Table 1). Therefore, the stronger WNPAC intensity for the moderate El Niño under the weakened THC implies alternative factor(s) influencing the strength of WNPAC.

Actually, the sensitivity of summertime WNPAC to the wintertime El Niño is enhanced under the weakened THC, beside the intensification of El Niño amplitude. The correlation coefficient between JA-mean WNPAC and DJF-mean Niño 3 is 0.24 in the 1 Sv (being significant at 98% confidence level by t test), but -0.03 in the CNTL. There are 70% El Niño events that (14 out of 20) are associated with WNPAC in the 1 Sv, compared to 62.7% (89 out of 142) in the CNTL. Additionally, the enhanced sensitivity of summertime WNPAC to the El Niño in the 1 Sv also can be demonstrated by the facts that not only the strength of WNPAC associated with moderate El Niño in the 1 Sv ($0.80 \times 10^6 \, m^2 \, s^{-1}$; Figure 10c) is comparable to that associated with the strong El Niño in the CNTL ($0.86 \times 10^6 \, m^2 \, s^{-1}$; Figure 9f) but also the anomalous anticyclonic circulation associated with moderate El Niño in the 1 Sv is concentrated over the WNP (Figure 10c), compared to a southeastward shift associated with strong El Niño in the CNTL (Figure 9f). Furthermore, the WNPACs in D(0)JF(1)
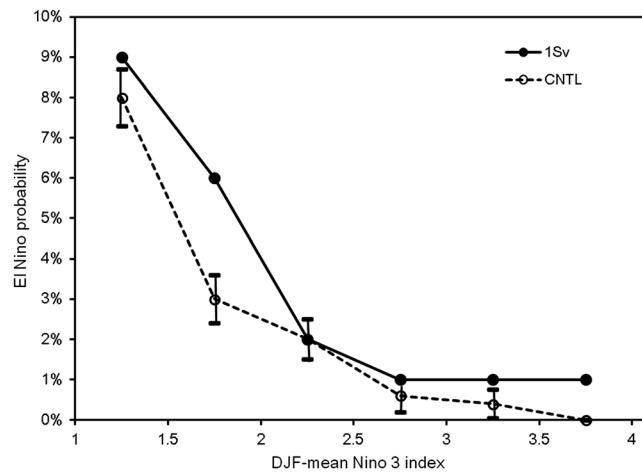

Figure 8. Probability distribution of DJF-mean Niño 3 index for the 1 Sv (solid line) and for the CNTL (dashed line). The probability represents the proportion of El Niño events with D(0)JF(1) Niño 3 indices in various strength bins among all integration years. The black bars represent the spread among the 100 years segments in the 1000 years CNTL.

Table 1. Values of December (D; 0)-January-February (JF; 1) Niño 3 Index (°C) for Various Categories of El Niño Events

El Niño Events	1 Sv (Cases)	CNTL (Cases)
All	1.80°C (20)	1.64°C (142)
Strong	2.80°C (5)	2.46°C (33)
Moderate	1.43°C (15)	1.39°C (109)

and MAM(1) in the 1 Sv is relatively weaker than those in the CNTL (Figures 4 and 9), although the strength El Niño is stronger in the 1 Sv than that in the CNTL. Therefore, for the intensified summertime WNPAC in the 1 Sv, particularly associated with moderate El Niño, the enhanced sensitivity of WNPAC to the El Niño might play a more important role than the increased El Niño amplitude.

Figure 11a shows the changes of climatological mean specific humidity in JJA between the 1 Sv and the CNTL. The specific humidity increased from the western to the central North Pacific and decreased in other regions in the Northern Hemisphere. The enhanced specific humidity over the western to central North Pacific is associated with positive SST (Figure 1c) and precipitation anomalies in that region, and the former is caused by lower tropospheric moisture convergence [*Lu and Dong*, 2008]. Furthermore, under the background of enhanced specific humidity over the western to central
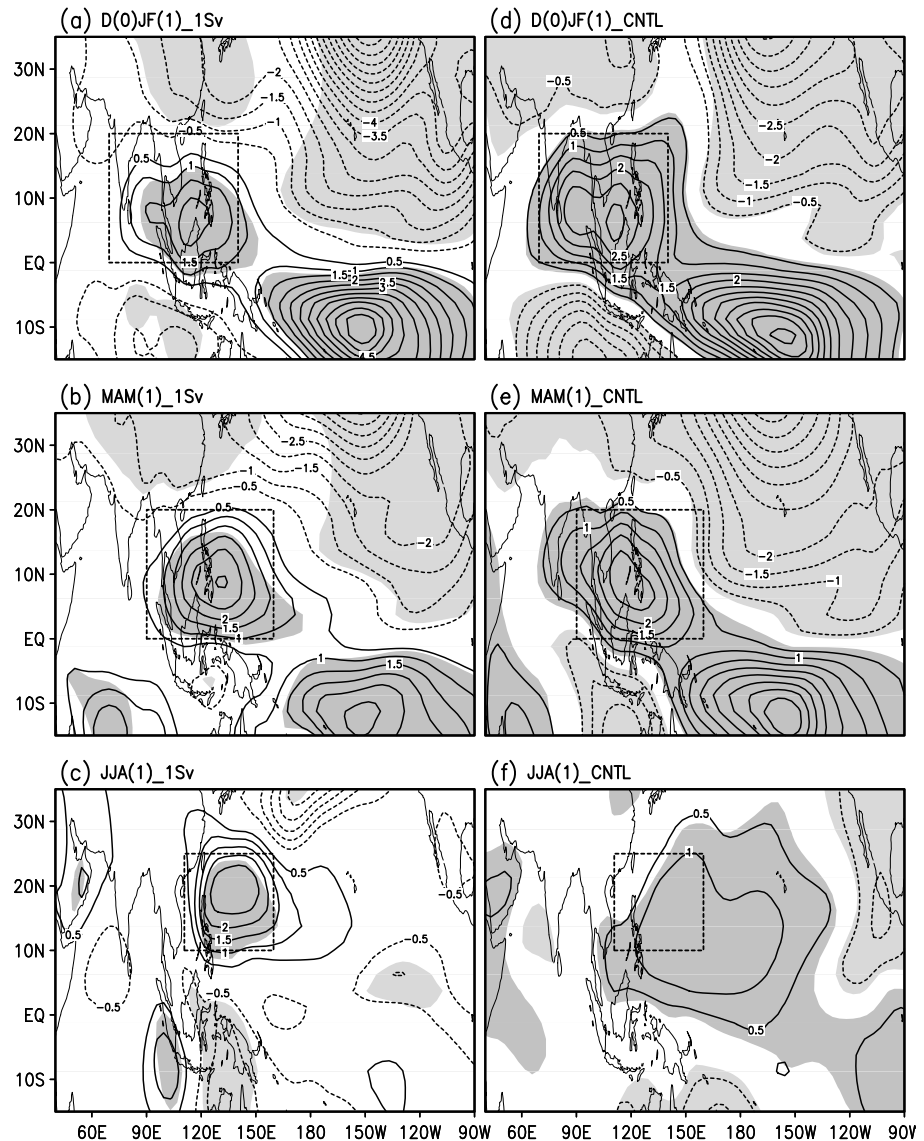

Figure 9. Same as Figure 4 but for the strong El Niño events (with D(0)JF(1) Niño 3 index greater than 2.0°C).
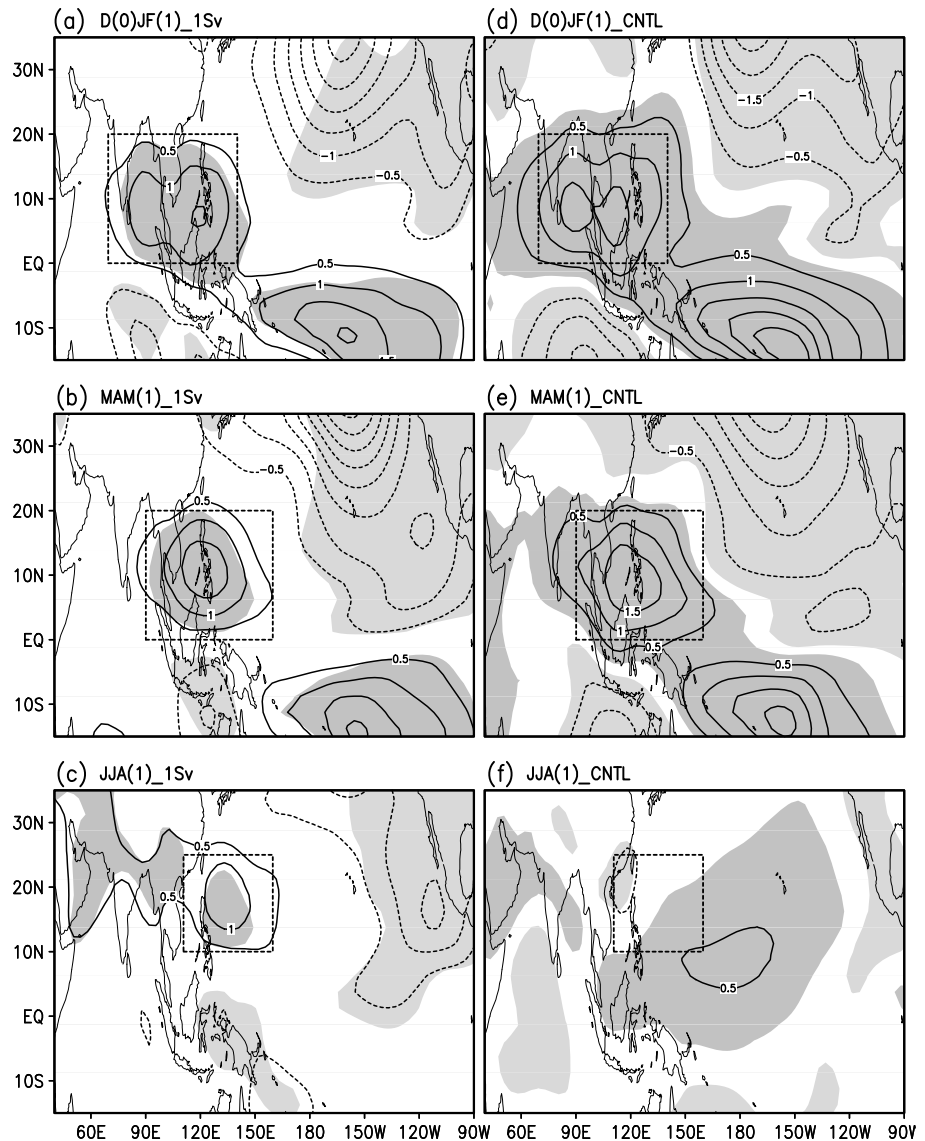
Figure 10. Same as Figure 4 but for the moderate El Niño events (with D(0)JF(1) Niño 3 index greater than 1.0°C but less than 2.0°C).

North Pacific, the interannual variability of the precipitation anomaly in that region is intensified (Figure 11b) because the enhancement of specific humidity increases the sensitivity of moisture convection [e.g., *Derbyshire et al.*, 2004]. In addition, the WNP is the mean convergence region resulting from the relatively warm water and is thus favorable for amplifying the atmospheric responses over the WNP [*Hong et al.*, 2013].

Figure 11c shows the difference of interannual standard deviation for the 850 hPa stream function between the 1 Sv and the CNTL. The interannual variation of lower tropospheric circulation anomalies showed a significant enhancement over the WNP and the northeast Pacific. The enhancement of circulation variability over the WNP can be explained by the stronger variability in diabatic heating induced by the precipitation anomaly over the central North Pacific, according to the Gill pattern (Figure 11b). Therefore, although the intensity of moderate El Niño events is quite similar between the 1 Sv and the CNTL, the corresponding summertime WNPACs can still be intensified under the weakened THC due to enhanced climatological specific humidity and resultant intensified precipitation variability. In addition, the changes in the specific humidity anomaly over the western to central North Pacific associated with El Niño were amplified in the 1 Sv
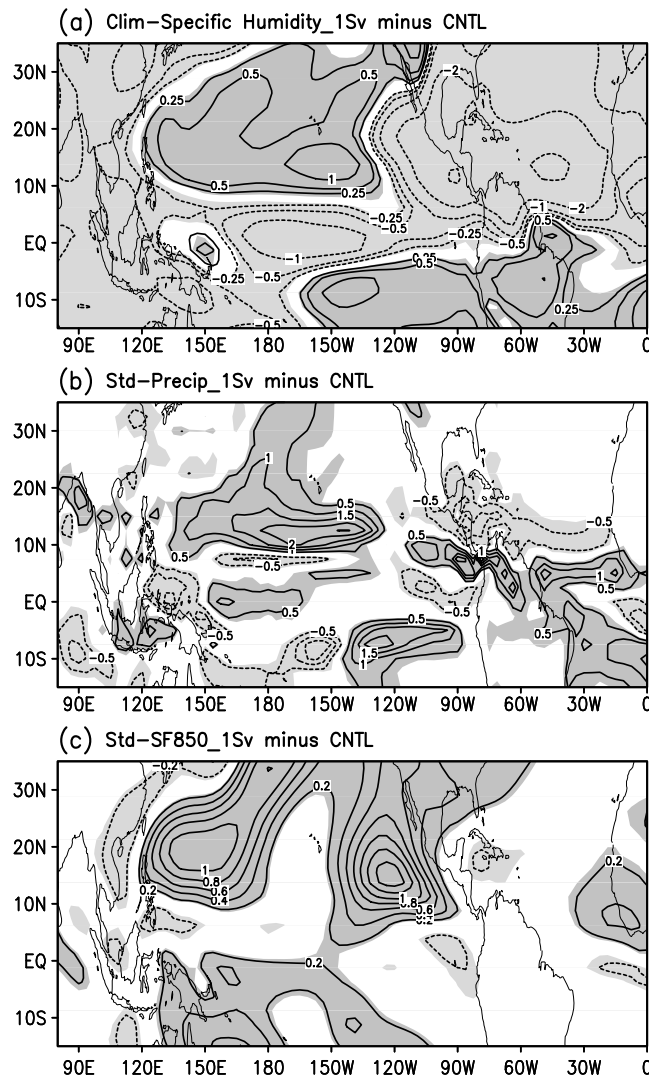
Figure 11. Differences of (a) climatological mean specific humidity (g kg^{-1}), (b) interannual standard deviation of precipitation (mm d^{-1}), and (c) 850 hPa stream function (10^6 m^2 s^{-1}) in JJA between the 1 Sv and the CNTL. Shading indicates differences significant at the 95% confidence level according to the *t* test for Figure 11a and the *F* test for Figures 11b and 11c.

compared with those in the CNTL (not shown), leading to enhanced positive feedback between convection and circulation over this region.

In addition, the sufficient climatological humidity is a necessary condition for the occurrence of strong circulation variability over the WNP, because of a positively coupled feedback between circulation and convection over the WNP [*Kosaka et al.*, 2013]. The WNPAC is a cold Rossby wave response to precipitation decrease. Moreover, the associated easterly on the southern flank reduces surface evaporation and further suppresses the precipitation. Even though the SST forcing is similar between the 1 Sv and CNTL, the increase of mean state humidity under the weakened THC contributes to a stronger variability of circulation and convection than that in the CNTL.

The enhancement of climatological humidity over the western to central North Pacific responsible for the intensification of El Niño-induced WNPAC under the weakened THC was deduced from analysis of the moderate El Niño events. However, it can be estimated that this mechanism can also be applied to the strong El Niño events.

6. Concluding Remarks

In this study, the response of WNPAC during the El Niño decaying summer to the weakened THC is investigated by comparing the results of a 1 Sv water-hosing experiment with those of the CNTL. The results suggest that the WNPAC is intensified under the background of weakened THC. The strength of the summertime WNPAC was more than 4 times as strong as that for the CNTL. In addition, the strength of WNPAC for the 1 Sv was stronger than any of the 100 years segments in the 1000 years CNTL, which further indicates a robust intensification of WNPAC during El Niño decaying summers by the weakened THC. In addition, the precipitation anomalies over the WNP in the El Niño decaying summer also intensified under the weakened THC, which is associated with enhancement of the WNPAC in the 1 Sv.

The strengthened wintertime El Niño by the weakened THC contributes to the strong summertime WNPAC in the 1 Sv experiment. On the one hand, the intensity of wintertime El Niño and the frequency of strong El Niño events were increased in the 1 Sv. On the other hand, the probability of WNPAC occurrence was increased along with the strengthening of wintertime El Niño intensity, which means that a strong wintertime El Niño tends to be followed by a strong summertime WNPAC. Thus, the intensified El Niño by the weakened THC results in a strengthened WNPAC in the following summer.

Moreover, the sensitivity of summertime WNPAC to the preceding wither El Niño is also enhanced under the weakened THC. The positive relationship between WNPAC and Niño 3 becomes quite weak during summer in the CNTL but still maintains in the 1 Sv. The result indicates that not only the El Niño is stronger in the 1 Sv than that in the CNTL but also the sensitivity of WNPAC to the El Niño is larger in the 1 Sv than that in the CNTL.

The present study further suggests that the enhanced sensitivity of summertime WNPAC to the El Niño is due to the increased climatological specific humidity in the lower troposphere over the western to central North Pacific as a response to the weakened THC. The increase of mean state specific humidity provides favorable conditions for the development of convection activities, which intensifies the interannual variability of precipitation over the central North Pacific, and therefore the variability of circulation over the WNP. This mechanism, although applied to the strong El Niño events, can be particularly useful for explaining the WNPAC intensification for the moderate El Niño events, because such events did not exhibit appreciable changes in intensity between the 1 Sv and the CNTL.

The model results support the observed evidence such that the multidecadal variability of the El Niño-WNPAC relationship is consistent with the low-frequency fluctuation of the AMO. Furthermore, the physical mechanism addressed by the model indicates that the modulation of AMO to the El Niño-WNPAC relationship can be explained by the multidecadal variability of El Niño intensity and the climatological specific humidity over the WNP, which also supports the hypothesis proposed in observations. Thus, both the model and the observational results indicate the role of Atlantic SST in the El Niño-WNP summer monsoon relationship. The mechanisms revealed by the model experiments offer an explanation for the observed evidence.

It should be noted that on the decadal timescale, *Chowdary et al.* [2012] mentioned a modulation of Pacific decadal oscillation (PDO) to the ENSO variability, similar to AMO. The relationship between the PDO index and standard deviation of the Niño 3 index was also checked (not shown). The results indicated that the correlation between PDO and ENSO variance is not stable for long-term period. From the 1930s to the 1960s, the PDO had a negative correlation with ENSO variance. From the 1970s to the 1990s, however, the PDO began to show a positive correlation with ENSO variance. Therefore, on the multidecadal timescale, the AMO is strongly associated with multidecadal fluctuation of the ENSO variance [e.g., *Dong et al.*, 2006; *Timmermann et al.*, 2007].

References

AchutaRao, K., and K. Sperber (2002), Simulation of the El Niño Southern Oscillation: Results from the coupled model intercomparison project, *Clim. Dyn.*, *19*, 191–209.

Chang, C. P., Y. S. Zhang, and T. Li (2000), Interannual and interdecadal variations of the East Asian summer monsoon and tropical Pacific SSTs. Part I: Roles of the subtropical ridge, *J. Clim.*, *13*, 4310–4325, doi:10.1175/1520-0442(2000)0132.0.CO;2.

Chen, W., J.-K. Park, B.-W. Dong, R.-Y. Lu, and W.-S. Jung (2012), The relationship between ENSO and the western North Pacific summer climate in a coupled GCM: Role of the duration of El Niño decaying phases, *J. Geophys. Res.*, *117*, D12111, doi:10.1029/2011JD017385.

Chou, C., J.-Y. Tu, and J.-Y. Yu (2003), Interannual variability of the western North Pacific summer monsoon: Differences between ENSO and non-ENSO years, *J. Clim.*, *16*, 2275–2287, doi:10.1175/2761.1.

Chowdary, J. S., S.-P. Xie, J.-Y. Lee, Y. Kosaka, and B. Wang (2010), Predictability of summer Northwest Pacific climate in 11 coupled model hindcasts: Local and remote forcing, *J. Geophys. Res.*, *115*, D22121, doi:10.1029/2010JD014595.

Chowdary, J. S., S.-P. Xie, J.-J. Luo, J. Hafner, S. Behera, Y. Masumoto, and T.Yamagata (2011), Predictability of Northwest Pacific climate during summer and the role of the tropical Indian Ocean, *Clim. Dyn.*, *36*(3–4), 607–621.

Chowdary, J. S., S.-P. Xie, H. Tokinaga, Y. M. Okumura, H. Kubota, N. C. Johnson, and X.-T. Zheng (2012), Interdecadal variations in ENSO teleconnection to the Indo-western Pacific for 1870–2007, *J. Clim.*, *25*(5), 1722–1744, doi:10.1175/JCLI-D-11-00070.1.

Chowdary, J. S., H. S. Chaudhari, C. Gnanaseelan, A. Parekh, A. Suryachandra Rao, P. Sreenivas, S. Pokharel, and P. Singh (2014), Summer monsoon circulation and precipitation over the tropical Indian Ocean during ENSO in the NCEP climate forecast system, *Clim. Dyn.*, doi:10.1007/s00382-013-1826-5.

Collins, M., S. F. B. Tett, and C. Cooper (2001), The internal climate variability of HadCM3, a version of the Hadley Centre coupled model without flux adjustments, *Clim. Dyn.*, *17*, 61–81.

Compo, G. P., et al. (2011), The twentieth century reanalysis project, *Q. J. R. Meteorol. Soc.*, *137*, 1–28, doi:10.1002/qj.776.

Dahl, K. A., A. J. Broccoli, and R. J. Stouffer (2005), Assessing the role of North Atlantic freshwater forcing in millennial scale climate variability: A tropical Atlantic perspective, *Clim. Dyn.*, *24*, 325–346, doi:10.1007/s00382-004-0499-5.

Derbyshire, S. H., I. Beau, P. Bechtold, J.-Y. Grandpeix, J.-M. Pirou, J.-L. Redelsperger, and P. Soares (2004), Sensitivity of moist convection to environmental humidity, *Q. J. R. Meteorol. Soc.*, *130*, 3055–3079.

Ding, R., K.-J. Ha, and J. Li (2010), Interdecadal shift in the relationship between the East Asian summer monsoon and the tropical Indian Ocean, *Clim. Dyn.*, *34*, 1059–1071, doi:10.1007/s00382-009-0555-2.

Dong, B., and R. Sutton (2002), Adjustment of the coupled ocean-atmosphere system to a sudden change in the thermohaline circulation, *Geophys. Res. Lett.*, *29*(15), 1728, doi:10.1029/2002GL015229.

Dong, B., and R. T. Sutton (2007), Enhancement of ENSO variability by a weakened Atlantic thermohaline circulation in a coupled GCM, *J. Clim.*, *20*, 4920–4939, doi:10.1175/JCLI4284.1.

Dong, B., R. T. Sutton, and A. A. Scaife (2006), Multidecadal modulation of El Niño-Southern Oscillation (ENSO) variance by Atlantic Ocean sea surface temperatures, *Geophys. Res. Lett.*, *33*, L08705, doi:10.1029/2006GL025766.

Gordon, C., C. Cooper, C. A. Senior, H. Banks, J. M. Gregory, T. C. Johns, J. F. B. Mitchell, and R. A. Wood (2000), The simulation of SST, sea ice extents and ocean heat transports in a version of the Hadley Centre coupled model without flux adjustments, *Clim. Dyn.*, *16*, 147–168.

Gu, D., and S. G. H. Philander (1995), Secular changes of annual and interannual variability in the Tropics during the past century, *J. Clim.*, *8*, 864–876, doi:10.1175/1520-0442(1995)2.0.CO;2.

Hong, S., I.-S. Kang, I.-D. Choi, and Y.-G. Ham (2013), Climate responses in the tropical pacific associated with Atlantic warming in recent decades, *Asia-Pac. J. Atmos. Sci.*, *49*(2), 209–217, doi:10.1007/s13143-013-0021-2.

Joseph, R., and S. Nigam (2006), ENSO evolution and teleconnections in IPCC's twentieth-century climate simulations: Realistic representation?, *J. Clim.*, *19*, 4360–4377.

Kalnay, E., et al. (1996), The NCEP/NCAR 40-year reanalysis project, *Bull. Am. Meteorol. Soc.*, *77*, 437–471.

Kosaka, Y., S.-P. Xie, N.-C. Lau, and G. A. Vecchi (2013), Origin of seasonal predictability for summer climate over the northwestern Pacific, *Proc. Natl. Acad. Sci. U.S.A.*, *110*, 7574–7579, doi:10.1073/pnas.1215582110.

Lau, N. C., and M. J. Nath (2006), ENSO modulation of the interannual and intraseasonal variability of the East Asian monsoon—A model study, *J. Clim.*, *19*, 4508–4530, doi:10.1175/JCLI3878.1.

Li, S., J. Lu, G. Huang, and K. Hu (2008), Tropical Indian Ocean basin warming and East Asian summer monsoon: A multiple AGCM study, *J. Clim.*, *21*, 6080–6088, doi:10.1175/2008JCLI2433.1.

Li, S. L., J. Perlwitz, M. P. Hoerling, and X. T. Chen (2010), Opposite annular responses of Northern and Southern Hemisphere to Indian Ocean warming, *J. Clim.*, *23*(13), 3720–3738.

Li, Y., R. Lu, and B. Dong (2007), The ENSO-Asian monsoon interaction in a coupled ocean-atmosphere GCM, *J. Clim.*, *20*, 5164–5177, doi:10.1175/JCLI4289.1.

Lu, R. (2001), Interannual variability of the summertime North Pacific subtropical high and its relation to atmospheric convection over the warm pool, *J. Meteorol. Soc. Jpn.*, *79*, 771–783, doi:10.2151/jmsj.79.771.

Lu, R., and B. Dong (2001), Westward extension of North Pacific subtropical high in summer, *J. Meteorol. Soc. Jpn.*, *79*, 1229–1241, doi:10.2151/jmsj.79.1229.

Lu, R., and B. Dong (2008), Response of the Asian summer monsoon to a weakening of Atlantic thermohaline circulation, *Adv. Atmos. Sci.*, *25*, 723–736, doi:10.1007/s00376-008-0723-z.

Lu, R., W. Chen, and B. Dong (2008), How does a weakened Atlantic thermohaline circulation lead to an intensification of the ENSO-South Asian summer monsoon interaction?, *Geophys. Res. Lett.*, *35*, L08706, doi:10.1029/2008GL033394.

Pope, V. D., M. L. Gallani, P. R. Rowntree, and R. A. Stratton (2000), The impact of new physical parameterizations in the Hadley Centre climate model: HadAM3, *Clim. Dyn.*, *16*, 123–146.

Rayner, N. A., D. E. Parker, E. B. Horton, C. K. Folland, L. V. Alexander, D. P. Rowell, E. C. Kent, and A. Kaplan (2003), Global analyses of SST, sea ice and night marine air temperature since the late nineteenth century, *J. Geophys. Res.*, *108*(D14), 4407, doi:10.1029/2002JD002670.

Stouffer, R. J., et al. (2006), Investigating the causes of the response of the thermohaline circulation to past and future climate changes, *J. Clim.*, *19*, 1365–1387.

Stuecker, M. F., A. Timmermann, F.-F. Jin, S. McGregor, and H.-L. Ren (2013), A combination mode of the annual cycle and the El Niño/Southern Oscillation, *Nat. Geosci.*, *6*, 540–544, doi:10.1038/ngeo1826.

Sutton, R. T., and D. L. R. Hodson (2007), Climate response to basin-scale warming and cooling of the North Atlantic Ocean, *J. Clim.*, *20*, 891–907, doi:10.1175/JCLI4038.1.

Timmermann, A., S. An, U. Krebs, and H. Goosse (2005), ENSO suppression due to a weakening of the North Atlantic thermohaline circulation, *J. Clim.*, *18*, 3122–3139.

Timmermann, A., et al. (2007), The influence of a weakening of the Atlantic meridional overturning circulation on ENSO, *J. Clim.*, *20*, 4899–4919.

Wang, B., and S.-I. An (2002), A mechanism for decadal changes of ENSO behavior: Roles of background wind changes, *Clim. Dyn.*, *18*, 475–486, dio:10.1007/s00382-001-0189-5.

Wang, B., R. G. Wu, and X. H. Fu (2000), Pacific-East Asian teleconnection: How does ENSO affect East Asian climate?, *J. Clim.*, *13*, 1517–1536, doi:10.1175/1520-0442(2000)0132.0.CO;2.

Wang, B., J. Yang, T. Zhou, and B. Wang (2008), Interdecadal changes in the major modes of Asian-Australian monsoon variability: Strengthening relationship with ENSO since the late 1970s, *J. Clim.*, *21*, 1771–1789, doi:10.1175/2007JCLI1981.1.

Watanabe, M., and F.-F. Jin (2002), Role of Indian Ocean warming in the development of Philippine Sea anticyclone during ENSO, *Geophys. Res. Lett.*, *29*(10), 1478, doi:10.1029/2001GL014318.

Wu, R., and B. Wang (2002), A contrast of the East Asian summer monsoon-ENSO relationship between 1962-77 and 1978-93, *J. Clim.*, *15*(22), 3266–3279, doi:10.1175/1520-0442(2002)0152.0.CO;2.

Wu, R., Z.-Z. Hu, and B. P. Kirtman (2003), Evolution of ENSO related rainfall anomalies in East Asia, *J. Clim.*, *16*, 3742–3758, doi:10.1175/1520-0442(2003)0162.0.CO;2.

Xie, S.-P., K. Hu, J. Hafner, H. Tokinaga, Y. Du, G. Huang, and T. Sampe (2009), Indian Ocean capacitor effect on Indo-Western Pacific climate during the summer following El Niño, *J. Clim.*, *22*, 730–747, doi:10.1175/2008JCLI2544.1.

Xie, S.-P., Y. Du, G. Huang, X.-T. Zheng, H. Tokinaga, K. Hu, and Q. Liu (2010), Decadal shift in El Niño influences on Indo-Western Pacific and East Asian climate in the 1970s, *J. Clim.*, *2*, 3352–3368, doi:10.1175/2010JCLI3429.1.

Yang, J., Q. Liu, S.-P. Xie, Z. Liu, and L. Wu (2007), Impact of the Indian Ocean SST basin mode on the Asian summer monsoon, *Geophys. Res. Lett.*, *34*, L02708, doi:10.1029/2006GL028571.

Yin, X., B. E. Gleason, G. P. Compo, N. Matsui, and R. S. Vose (2008), The International Surface Pressure Databank (ISPD) land component version 2.2, Natl. Clim. Data Cent., Asheville, N. C. [Available at ftp://ftp.ncdc.noaa.gov/pub/data/ispd/doc/ISPD2_2.pdf.]

Zhang, R., and T. L. Delworth (2005), Simulated tropical response to a substantial weakening of the Atlantic thermohaline circulation, *J. Clim.*, *18*, 1853–1860, doi:10.1175/JCLI3460.1.